

Design of an aeroelastically tailored wind turbine blade tip for field experiments



Energy & Materials Transition www.tno.nl +31 88 866 50 65 info@tno.nl

TNO 2025 R10229 - 30 January 2025
Design of an aeroelastically
tailored wind turbine blade tip for
field experiments

Author(s) E. Fritz, K. Boorsma, A. Herrig (LM Wind Power)

Classification report TNO Public

Number of pages 24 (excl. front and back cover)

Number of appendices 0

Sponsor This contribution has been financed with Topsector Energiesubsidie

from the Dutch Ministry of Economic Affairs under grant no.

TEHE119018.

Project name TIADE
Project number 060.39674

) TNO Public) TNO 2025 R10229

All rights reserved

No part of this publication may be reproduced and/or published by print, photoprint, microfilm or any other means without the previous written consent of TNO.

©2025 TNO

Summary

This report explores the impact of a swept wind turbine blade tip on extreme and fatigue blade and tower loading through numerical investigations. These are conducted within the context of the TIADE project, a field experiment on a 3.8 MW research turbine, which planned a campaign with segmented blades that allow the application of alternative tip geometries. Within the available tip design space, dictated by the position and allowable load of a blade tip joint, the maximum allowable tip sweep is determined.

Based on aeroelastic simulations of design load cases 1.2 and 1.3 according to IEC standard 61400-1, the sweep-induced changes to fatigue and extreme loads at blade root, tip joint and tower bottom are evaluated. It is demonstrated that a reduction in flapwise blade root extreme loads and lifetime damage-equivalent loads of 1.0% and 2.6%, respectively, can be achieved when compared against a straight reference blade. At the tip joint, the relative flapwise load reductions are even larger. Torsional loads are shown to also decrease at the blade root but increase in the sweep part of the blade where the coupling of bending and torsional deformations due to sweep is strongest. Edgewise loads are largely insensitive to sweeping the blade tip. Tower bottom loads also decrease, with fore-aft extreme and damage equivalent fatigue loads exhibiting the most pronounced relative reductions of 1.6% and 2.1%, respectively. Finally, the rotor performance is shown to hardly be affected by blade sweep.

By performing this analysis in the framework of a field experiment, the relevance of the results for full-scale wind turbine blades is ensured. The outcomes corroborate the potential of swept tips as retrofit options for segmented blades or as a design choice for novel blades with decreased weight and cost.

TNO Public 3/24

Contents

Sumi	mary	3
Conte	ents	4
List c	of tables and figures	5
Nom	enclature	6
1	Introduction	7
2	Methodology	g
2.1	Limitations imposed by the project	9
2.2	Working principle of blade sweep	<u>C</u>
2.3	Numerical modelling	11
3	Results	12
3.1	Crossflow-corrected versus fully-corrected BEM simulations	
3.2	Application of steady twist compensation	
3.3	Determination of the allowable sweep extent	14
3.4	Effect of blade sweep on extreme loads	14
3.5	Effect of blade sweep on fatigue loads	17
3.6	Effect of blade sweep on energy production	19
4	Conclusions and outlook	21
Refer	rences	23

List of tables and figures

_		
10	h	Δc
ıυ	U	

3.1	Relative difference in C_T between the fully sweep-corrected and
3.2 3.3	crossflow-corrected simulations
Figure	es ·
2.1 2.2	Schematic of the crossflow principle
3.1	Relative difference in axial induction factor (a) and normal force (b) between simulations fully corrected for blade sweep (subscript Λ) and those corrected for cross-
3.2	flow only (subscript cf)
3.3	Ratio of the extreme torsional moment at the tip joint for blade tips of varying sweep extent operating with reduced rated rotor speed Ω^* and the straight reference tip operating with original rated rotor speed Ω^0
3.4	Schematic representation of a wind turbine blade with a swept tip defined by $z_{start}/R=0.8$ and $y_{tip}/R=-0.02$, blade planform based on the IEA 15 MW
3.5	reference wind turbine [25]
3.6	Correlation of torsional and flapwise blade moments at blade root and tip joint for the straight and swept-bladed configuration
3.7	Normalised fore-aft, side-side and yaw extreme loads at the tower bottom as a
3.8	function of wind speed for the straight and swept case
3.9	a function of wind speed for the straight and swept case
3.10	of wind speed for the straight and swept case

TNO Public 5/24

Nomenclature

Latin letters	
AEP	Annual energy production
a	Axial induction factor
c	Chord
c_l	Lift coefficient
DEL	Damage-equivalent load
DLC	Design load case
F	Probability of wind speeds
F_N	Rotor plane normal force
F_x, F_y	Chord normal and tangential forces
L	Lift force
M_f, M_e, M_t	Flapwise, edgewise and torsional blade moment
M_{fa}, M_{ss}, M_{yaw}	Fore-aft, side-side and yawing tower moment
m	Wöhler exponent
N_{ref}	Number of reference cycles
P	Power
R	Blade tip radius
r_P	Pearson correlation coefficient
s_a, s_b	Arbitrary signals
U_{ave}	Average free stream velocity according to IEC standard 61400-1
U_{∞}	Freestream velocity
u, v	Velocity components
V	Local inflow velocity
V_{rot}	Rotational velocity
y_{tip}	Tip sweep
z_{start}	Sweep starting position

Greek letters	
α	Angle of attack
β	Pitch angle
β_{twist}	Twist angle
ζ	Global sweep angle
Λ	Local sweep angle
ρ	Density of air
Ω^0	Original rated rotor speed
Ω^*	Reduced rated rotor speed
Subscripts	
cf	Corrected for crossflow
Λ	Corrected for crossflow, trailed vorticity displacement and bound vortex self-induction

TNO Public 6/24

1 Introduction

The blades of horizontal axis wind turbines (HAWT) have grown beyond 100 m blade span. These increasingly slender and flexible structures necessitate a detailed aeroelastic analysis [1]. Simultaneously, concepts for aeroelastic tailoring of the blades' properties become ever more relevant. One solution for tailoring the aeroelastic characteristics of a wind turbine blade is gradually sweeping the blade axis in the rotor plane. By doing so, bending and torsion deformations are coupled, which can be exploited to reduce extreme and fatigue blade loading.

In the past, swept blades were experimentally tested in the STAR (Sweep Twist Adaptive Rotor) project. Initial investigations by Zuteck [2] and Larwood and Zuteck [3] demonstrated the possibility for a sweep-induced increase in torsional deformation and a decrease in flapwise deformation, respectively. The swept blades eventually implemented in the field had a slightly extended blade length compared to their straight baseline. They showed an improved annual energy production of $10-12\,\%$ while maintaining the load envelope of the 750 kW reference wind turbine with straight blades [4].

More recently, Barlas et al. [5] conducted a numerical blade tip design optimisation study aimed at maximising power under ultimate load constraints, resulting in a tip extension combining sweep and dihedral. Additionally, the aerodynamic and aeroelastic characteristics of a swept wind turbine blade tip were investigated experimentally in a wind tunnel [6] and on a rotating test rig in the field [7]. Fritz et al. studied the aerodynamics of a rotating model HAWT equipped with swept blades in a wind tunnel [8]. Such experimental efforts are partially motivated by the fact that low-fidelity numerical models generally used in the design and optimisation stages of wind turbine blades need to be validated in their ability to simulate such complex geometries accurately. Various efforts to assess and improve the accuracy of low-fidelity aerodynamic solvers for swept blades have been made [9, 10, 11, 12].

Given that blade sweep is motivated by its coupling of aerodynamic and structural effects, aeroelastic simulations are required to evaluate its benefits. Based on such simulations, Verelst and Larsen demonstrated that the flapwise extreme and fatigue loads at the blade root of the NREL 5 MW reference wind turbine could be reduced by up to 15% and 10%, respectively by sweeping the blade [13]. In contrast to that, the torsional extreme and fatigue loads increased up to 400% at the blade root. This increase in torsional moment is a significant drawback of swept blades and presumably a reason why this concept has not been adopted by manufacturers. A possible solution was presented by Hansen, who combined an aft sweep towards the tip with a forward sweep in the midboard region to compensate for the torsional loads [14]. The potential for lowering blade root flapwise fatigue loads was also found by Larwood et al. [15].

A possible conclusion of the above studies is that swept blade tips have significant potential as alternatives to straight blade tips for modular blades and as a conscious design choice in developing novel blades. There is, however, a lack of field research data confirming this potential on modern, multi-megawatt wind turbines.

The TIADE (Turbine Improvements for Additional Energy) project aims, among others, at the development of an aeroelastically tailored wind turbine blade tip for field application. In this joint research effort by TNO, GE Renewable Energy and LM Wind Power, field experiments are conducted on a 3.8 MW research wind turbine located in Wieringermeer, Netherlands. As part

TNO Public 7/24

of this research project's plan, unique jointed blades were developed that allow the exchange of the blade tip. The present work embodies the first step towards a field test of a swept blade tip on a wind turbine representative of the state-of-the-art. It details the numerical investigations conducted in the design phase of the aeroelastically tailored tip. The simulations give insight into sweep-induced changes in extreme and fatigue loading and annual energy production.

The remainder of this report is built up as follows: Section 2 details the limitations of the design space imposed by the considered blade geometry and its allowable load envelope, discusses the working principle of blade sweep, and introduces the numerical models used for this study. Section 3 opens with a discussion of modelling the purely aerodynamic impact of blade sweep, the need for compensation of steady twist deformations and the allowable sweep extent within load restrictions. Then, the sweep-induced changes in extreme loading, fatigue loading and annual energy production are presented. Conclusions are drawn in Section 4, and an outlook for future research is given.

TNO Public 8/24

2 Methodology

2.1 Limitations imposed by the project

In this research project, the tip design space is primarily limited by the location of the pin joint, which connects the blade tip with the inboard part of the blade and is located at 80% of the blade tip radius R. Thus, 20% R remain on which aeroelastic tailoring techniques can be applied. During the concept phase for the tip design, it was decided to tailor the blades' properties through bend-twist coupling. Bend-twist coupling achieved through off-axis fibre orientation, as discussed by Karaolis et al. [16] and Capellaro [17], was dismissed early on, as aeroelastic simulations indicated limited additional torsion deformation due to the insufficient blade length of the interchangeable tip. As an alternative to off-axis fibre orientation, bend-twist coupling can be achieved geometrically by sweeping the blade. Despite the limited design space, blade sweep can significantly impact the blades' aeroelastic behaviour, as will be shown in this article.

Another design limitation imposed by the pin joint is that it is designed for the load envelope of a conventional, straight blade tip. A swept blade tip, however, inevitably leads to an increase in torsional loads in some parts of the blade, particularly in the proximity of the swept region itself. A swept tip would, thus, likely exceed the pin joint's torsional load envelope. To solve this, the project partners proposed lowering the turbine's rated rotational speed. Consequently, a margin to the torsional load limit is opened, which can be filled up by the sweep-induced torsional loads. This will be discussed in more detail in Section 3.3. For potential future application of blade sweep to wind turbine blades, the locally increased torsional loads have to be considered in the design process, and the structural properties should be adjusted accordingly to withstand them. The numerical analyses presented in Sections 3.4 to 3.6 compare blade loading for a straight and swept blade, both operating at the reduced rated rotational speed. This allows the direct evaluation of the impact of blade sweep on wind turbine blade loads.

2.2 Working principle of blade sweep

2.2.1 Aerodynamic consequences of blade sweep

A major change in blade aerodynamics due to blade sweep is known as *crossflow principle*, see e.g. Hoerner [18]. For a straight blade, the local in-plane inflow velocity V is approximately perpendicular to the blade axis. However, if blade sweep is applied, this velocity is oriented at an angle that is a function of the global sweep angle ζ and the local sweep angle Λ , see Figure 2.1.

Considering the flow component $v=V\sin(\Lambda-\zeta)$, which is aligned with the local blade axis, equally large on the pressure and suction side of the airfoil, it has a negligible influence on the pressure forces. The local forces - lift, drag and pitching moment - are then a function of the in-plane velocity component perpendicular to the local blade axis $u=V\cos(\Lambda-\zeta)$. The angle of attack α as measured in the direction of u increases when compared to the angle of attack measured in alignment with V by $1/\cos(\Lambda-\zeta)$. Considering a constant lift slope $\partial c_l/\partial \alpha$, the local lift force per unit blade length $L=\frac{1}{2}\rho u^2cc_l$ becomes proportional to $\cos(\Lambda-\zeta)$. The same is true for the drag force and the pitching moment. At the same time, the infinitesimal blade

TNO Public 9/24

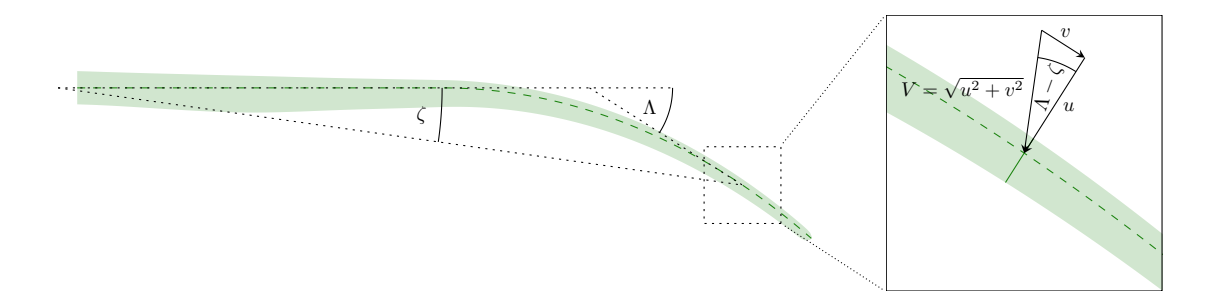


Figure 2.1: Schematic of the crossflow principle

length exceeds the corresponding infinitesimal radial length in the swept part of the blade by a factor of $1/\cos(\Lambda-\zeta)$. Therefore, the absolute blade forces, i.e. the sectional forces multiplied by the blade length, would be identical between straight and swept blades if not for further changes to the blade aerodynamics.

Considering a straight blade, its bound vorticity can be approximated by a straight vortex filament. Such a straight vortex filament does not induce a velocity on itself. If the blade is swept, however, the bound vorticity follows a curve and, thus, induces a velocity on itself. Additionally, the starting position of the trailed vorticity is displaced in azimuthal direction when compared to a straight reference blade. Considering that most of the vorticity is trailed in the dominant tip vortex, the changes in induction can be approximated by modelling the displacement of the tip vortex. The impact of these two phenomena is modelled numerically by Fritz et al. [11]. It should, however, be noted that a study by the same authors, validating the model using wind tunnel data, revealed that accounting only for the crossflow principle yielded approximately the same accuracy as when additionally modelling the effects mentioned above [19]. This validation study was conducted based on a wind tunnel model with exaggerated blade aftsweep, significantly exceeding the sweep cases discussed in this article. Section 3.1 discusses the impact of changes in the bound and trailed vortex system on the blade's aerodynamics.

2.2.2 Bend-twist coupling

From a structural viewpoint, blade sweep couples bending and torsional deformations. In operation, a section of a wind turbine blade experiences forces perpendicular and aligned with its chord line, F_x and F_y , respectively. These forces act at the aerodynamic centre, generally assumed to be at the quarter chord location. In conventional blade designs, the aerodynamic centre is sought to be close to the shear centre, defined as the location where an acting force will not induce a torsional deformation of the blade's regarded section. By sweeping the blade, the blade section, and thus its aerodynamic centre, is placed at a distance from its shear centre. As a consequence, the acting forces entail not only flapwise and edgewise deformations but also torsional deformations. The principle of bend-twist coupling is visualised in Figure 2.2.

When sweeping a blade forward, the sweep-induced torsion twists the cross-section to higher angles of attack. As long as the regarded cross-section is acting in the linear part of the lift curve, this increase in angle of attack is equivalent to higher loads. In contrast to that, aft sweep enforces a torsion to lower angles of attack, also referred to as twist to feather. In the linear region of the lift curve, this corresponds to lower loads on the blade section. Given that the design of the aeroelastically tailored tip is aimed at load reductions, only aft-swept geometries are considered in the present investigation.

TNO Public 10/24

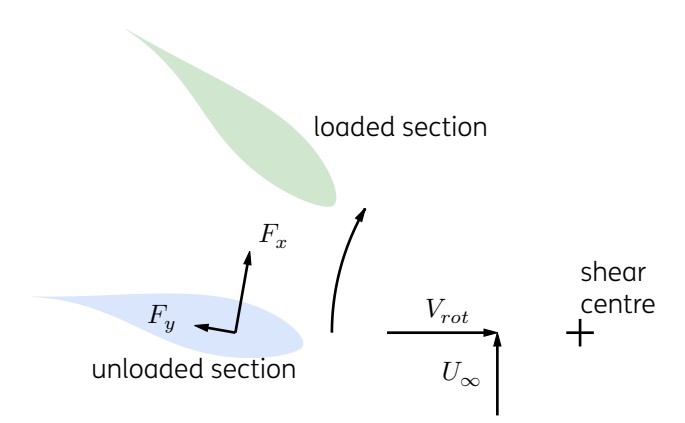


Figure 2.2: Schematic of the bend-twist coupling principle of swept blades, adapted from [3]

2.3 Numerical modelling

The simulations run for this study are based on two aerodynamic/aeroelastic tools, both based on blade element momentum theory (BEM):

- 1. A simple BEM algorithm based on the standard equations as presented e.g. in Burton et al. [20]. This code is purely aerodynamic and, thus, does not include blade deformations. For this study, a version of this code only accounting for crossflow and one additionally including the BEM correction model for swept blades [11] are implemented. In the remainder of this article, these two versions are denoted as crossflow-corrected and fully-corrected. Fritz et al. [11] validated the baseline version of this BEM algorithm against the established aerodynamic solver AWSM [21]. This tool is only used for a preliminary study presented in Section 3.1.
- 2. The BEM-based aeroelastic simulation tool PHATAS [22]. In the current PHATAS release 'JAN-2014a SuperV', the aforementioned BEM correction model is not included. This is shown to be of limited concern for the swept blade geometries considered in this study, see Section 3.1. Snel's first order dynamic stall model and correction model for three-dimensional flow are applied [23]. The aerodynamic solver is coupled to a non-linear structural dynamics solver, to take blade deformations into account while solving each time step. This tool allows the simulation of wind turbine design load cases (DLC) in accordance with IEC standard 61400-1 [24]. This tool is used for all simulations presented in Sections 3.2 to 3.6.

TNO Public 11/24

3 Results

Due to confidentiality agreements with the project partners GE Renewable Energy and LM Wind Power, the y-axes of the plots presented in this section are redacted or normalised. Nonetheless, they give clear indications regarding the influence of blade sweep on blade aerodynamics and aeroelasticity.

3.1 Crossflow-corrected versus fully-corrected BEM simulations

In an initial step, the influence of the BEM correction model for swept blades proposed by Fritz et al. [11] is evaluated. In a recent study, Fritz et al. aimed to validate the model using wind tunnel experimental data of blades with exaggerated sweep [19]. Despite the improved modelling of the occurring flow physics, the added benefit of this correction model was difficult to demonstrate. Simulations corrected only for crossflow matched the experimental results equally well as simulations fully corrected for sweep effects on blade aerodynamics.

To shed light on the relevance of this correction in the present study, the research turbine's blades are simulated both with only a crossflow correction (subscript cf) and fully corrected (subscript Λ). These simulations are run for swept blade tips with varying sweep extent y_{tip} , i.e. the maximum displacement of the blade axis in the rotor plane. All investigated tips follow a circular curve defined by the spanwise location of the tip joint (z_{start}) and the sweep extent at the tip (y_{tip}). The relative difference in the spanwise distributions of the axial induction factor and the normal force are shown in Figure 3.1.

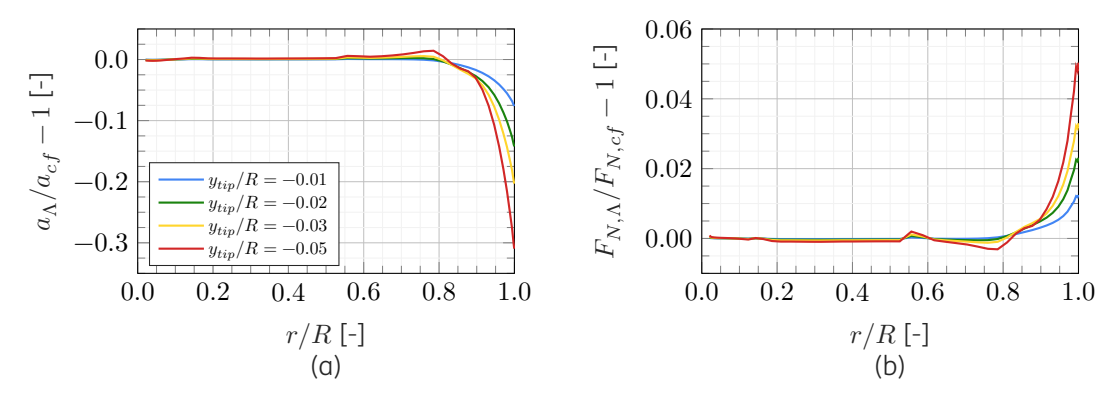


Figure 3.1: Relative difference in axial induction factor (a) and normal force (b) between simulations fully corrected for blade sweep (subscript Ω) and those corrected for crossflow only (subscript C = 0)

A seemingly significant relative difference in axial induction can be observed in the swept part of the blade (r/R>0.8). Given that the local inflow velocity in this region is dominated by its in-plane component V_{rot} , this difference in axial induction causes a much smaller relative difference in the local blade loading. This can be seen in Figure 3.1 (b), showing a slight increase in axial load at the tip when simulating with full sweep correction. It should be noted that outboard of approximately r/R=0.85, the normal force decreases rapidly so that relative differences in loading appear more prominent due to the diminishing denominator.

TNO Public 12/24

These differences in axial loading due to using the BEM correction model for swept blades are considered within reasonable limits, further supported by the relative difference in the rotor thrust coefficient C_T . For all simulated swept tips, the relative difference in thrust coefficient between the crossflow-corrected and fully-corrected BEM simulations is below $0.25\,\%$, see Table 3.1. Based on this observation, the BEM algorithm *Phatas*, which only corrects for crossflow, is deemed suitable for simulations of swept blades within the design space explored in this section.

Tip sweep y_{tip}	-0.01 R	-0.02 R	-0.03 R	-0.05 R
Relative difference in ${\cal C}_T$	+0.12 %	+0.19%	+0.23%	+0.23%

Table 3.1: Relative difference in C_T between the fully sweep-corrected and crossflow-corrected simulations

3.2 Application of steady twist compensation

Wind turbine blades have a twist distribution tailored to the expected aerodynamic inflow conditions. Additionally, the twist distribution accounts for the steady aeroelastic twist induced by the sectional moment coefficient during operation. Next to the airfoil pitching moment, blade sweep induces an additional elastic twist to the wind turbine blade. Two states can be distinguished: Elastic twist due to aerodynamic loading in steady wind conditions and twisting due to unsteady aerodynamic events such as a gust. Considering an aft-swept blade, it is clear that the steady aerodynamic loading of the swept part of the blade will induce a twist to lower angles of attack. Consequently, if one were to apply the same twist distribution to a swept blade as to a straight blade, the swept blade would experience lower aerodynamic forces and produce less power. Thus, a twist compensation should be applied, which corrects the operational angle of attack of the swept blade so that it more closely resembles that of the straight blade.

To determine the required twist compensation, aeroelastic simulations in steady wind are run for the straight and swept blade at approximately $1-2\,\mathrm{m/s}$ below the rated wind speed. This ensures that the twist compensation covers the larger twist deformations at rated conditions and the lower twist deformations for lower wind speeds equally well. Then, the difference in twist deformation between the swept and straight blade is added to the original blade's twist distribution as compensation. However, this could only be done in the region of the modular tip since the inboard blade geometry already existed. To ensure a smooth transition of the blade surface across the tip joint, the additional twist is faded out towards its location. Figure 3.2 depicts the original and amended twist distributions.

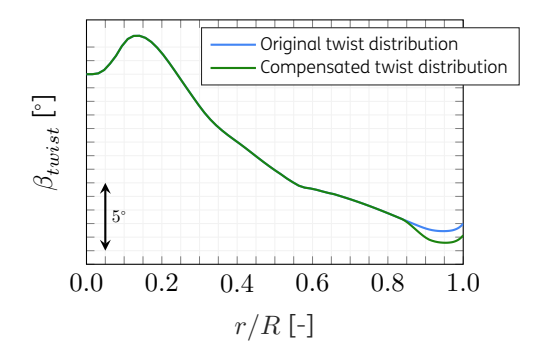


Figure 3.2: Twist distribution compensated for sweep-induced elastic deformations compared to the original twist distribution

TNO Public 13/24

3.3 Determination of the allowable sweep extent

As described in Section 2.1, a reduction in rated rotor speed is used to accommodate additional torsional loads at the tip joint caused by blade sweep. This reduction is enforced by changing the rated rotor speed in the simulation settings of the turbine controller, which adjusts the blade pitch angle accordingly. By comparing extreme torsional loads of the straight blade with the original rated rotor speed Ω^0 to those of the swept tip with reduced rated rotor speed Ω^* , it can be determined whether the tip joint's original load envelope is exceeded. Simulations with stepwise increasing wind speed were run to determine the relevant loads. Figure 3.3 shows the ratio of extreme torsional moments at the tip joint for blade tips with varying sweep extent. It can be observed that the torsional load limit is exceeded for a sweep extent larger than approximately two per cent of the blade radius.

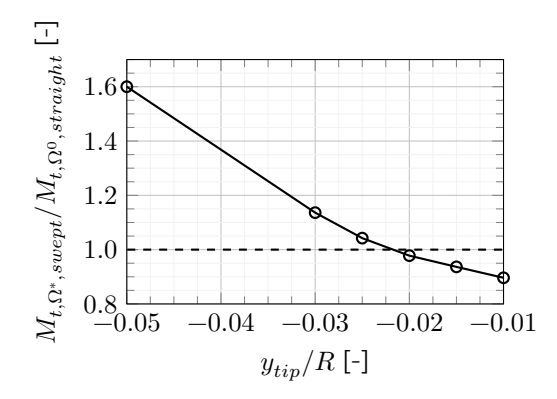


Figure 3.3: Ratio of the extreme torsional moment at the tip joint for blade tips of varying sweep extent operating with reduced rated rotor speed Ω^* and the straight reference tip operating with original rated rotor speed Ω^0

Combining this insight with the desire to maximise the impact of the swept blade tip, a design decision for a tip with a tip sweep of $y_{tip}/R=-0.02$ is made. Figure 3.4 gives a graphical representation of this swept tip defined by a sweep starting position of $z_{start}/R=0.8$ and a tip sweep of $y_{tip}/R=-0.02$.

Figure 3.4: Schematic representation of a wind turbine blade with a swept tip defined by $z_{start}/R=0.8$ and $y_{tin}/R=-0.02$, blade planform based on the IEA 15 MW reference wind turbine [25]

3.4 Effect of blade sweep on extreme loads

The effect of sweep on the extreme blade loads is determined by simulating operating conditions as defined by DLC 1.3 for turbine class IIB in IEC standard 61400-1 [24]. This DLC reflects the turbine in power production under extreme turbulence. Given that extreme loads are expected either around the rated conditions or around the cut-out wind speed, wind speeds between 8 m/s and 25 m/s are simulated. This assumption is supported by the results presented in this section. For each wind speed, twenty random wind seeds are simulated, and each simulation is 640 s long, of which the final 600 s are considered for this analysis to avoid the influence of start-up phenomena. The blade moments are investigated at two spanwise locations, namely at the blade root and tip joint. The blade root is commonly equipped with strain gauges in field experiments, which would offer data for validation. Furthermore, the tip joint is of interest both because it is the structurally most critical part of the research wind turbine blade and because it represents the starting position of the applied sweep. Next to the

TNO Public 14/24

aerodynamic moments on the blade, the moments acting on the base of the turbine tower are investigated.

For each random seed, the maximum flapwise, edgewise and torsional moments are determined and then averaged per wind speed. Figure 3.5 (a) – (c) shows the mean flapwise, edgewise and torsional blade root moment of both the straight and swept blade per wind speed. The general trends of all three moments agree well between the straight and swept blade simulations. The flapwise moment is closely related to the rotor thrust, which is typically highest at rated conditions before reducing for higher wind speeds. The edgewise and torsional blade root moments exhibit an approximately linear relation to the wind speed. With increasing wind speed, the occurring gust wind speeds also rise, leading to increased maximum loading in edgewise and torsional direction. Given that only the outer 20 % of the blade is swept, limited changes in blade root moments are observed. For most wind speeds, the flapwise and torsional loads of the straight blade slightly exceed those of the swept blade. The edgewise loads of the two blades almost coincide.

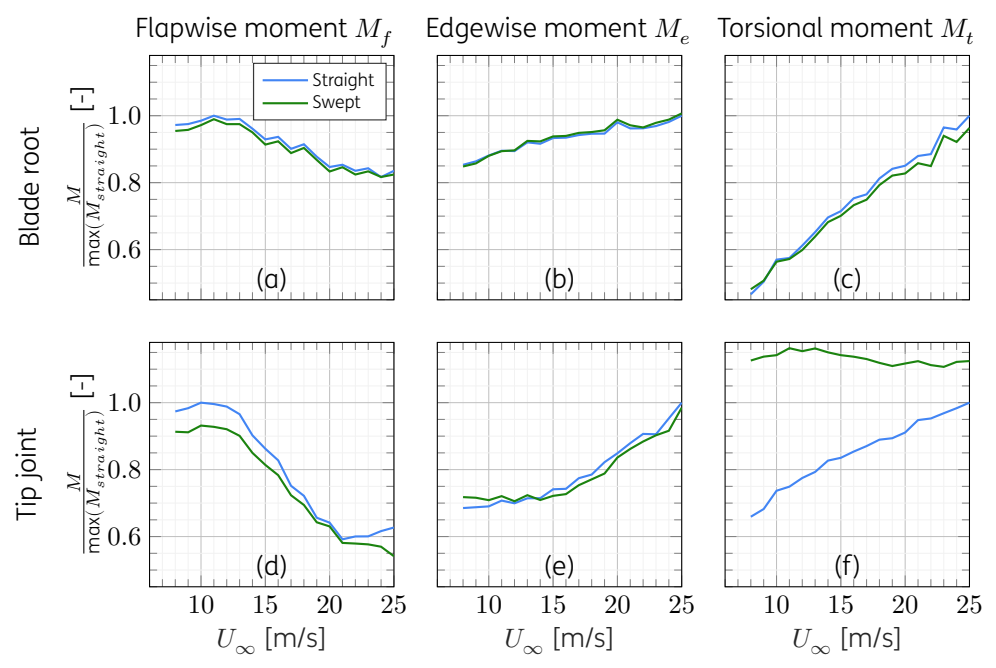


Figure 3.5: Normalised flapwise, edgewise and torsional extreme loads at the blade root and tip joint as a function of wind speed for the straight and swept case

Figure 3.5 (d) – (f) demonstrates the strong coupling effect of sweep at the tip joint. The swept blade exhibits lower flapwise loads throughout the operating range, with the highest reduction for lower wind speeds. At the same time, the torsional loads are increased considerably compared to the straight blade. While the torsional loads of the straight blade are close to proportional to the wind speed, the swept blade follows this trend only at the inboard location. At the tip joint, the torsional moment follows a trend more closely related to that of the flapwise moment, namely with a peak around rated and then a slight reduction with higher wind speeds. Again, the edgewise moment has little sensitivity to blade sweep.

To further demonstrate the coupling of flapwise bending and torsion, the correlation between the two output signals is calculated using the Pearson correlation coefficient. For two arbitrary signals s_a and s_b , this correlation coefficient is defined as

$$r_P = \frac{\sum (s_{a,i} - \bar{s}_a)(s_{b,i} - \bar{s}_b)}{\sqrt{\sum (s_{a,i} - \bar{s}_a)^2 \sum (s_{b,i} - \bar{s}_b)^2}}$$
(3.1)

TNO Public 15/24

Figure 3.6 shows the correlation of torsional and flapwise blade moments at the blade root and tip joint as a function of wind speed. At the blade root, the torsional and flapwise moment correlation is approximately equal for the straight and swept blade configurations. In contrast, the two moments are evidently more correlated at the tip joint for the swept blade than for the straight blade.

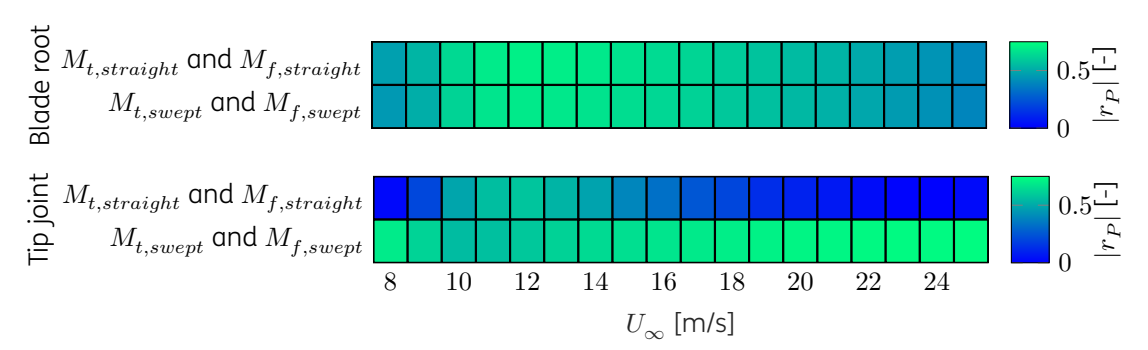


Figure 3.6: Correlation of torsional and flapwise blade moments at blade root and tip joint for the straight and swept-bladed configuration

The extreme tower bottom moments are shown in Figure 3.7. The fore-aft moment is closely related to the rotor thrust and flapwise blade moment and, thus, follows a comparable trend. Blade sweep reduces the tower fore-aft moment with a stronger decrease for low wind speeds. The side-side and yawing moments follow an approximately linear trend with increasing wind speed. Similar to the blade root edgewise and torsional moments, this can be explained by the existence of higher wind speed extrema with increasing wind speed. A slight sweep-induced decrease in the yawing moment can be observed, while the side-side moment barely changes.

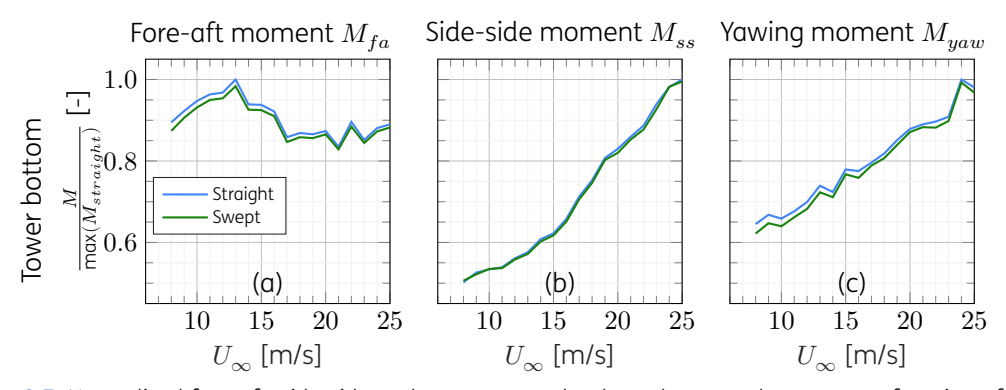


Figure 3.7: Normalised fore-aft, side-side and yaw extreme loads at the tower bottom as a function of wind speed for the straight and swept case

To summarise and quantify the effect of sweep on the blade and tower extreme loads, the relative difference in maximum moments experienced by the swept and straight blade configuration throughout DLC 1.3 are summed up in Table 3.2. Flapwise extreme loads reduce for both regarded spanwise locations. An even more substantial relative reduction can be observed for the torsional moment at the blade root, which comes with the penalty of a strong increase in torsion loads at the tip. In contrast to that, edgewise loads are barely affected, corroborating that blade sweep mostly couples flapwise and torsion deformations. All moments at the tower bottom are reduced when blade sweep is applied, with the largest decrease occurring in the fore-aft direction.

TNO Public 16/24

Location	ΔM_f	ΔM_e	ΔM_t
Blade root Tip joint	$\begin{array}{c c} -1.0\% \\ -6.8\% \end{array}$	$\left. \begin{array}{c} +0.7\% \\ -1.5\% \end{array} \right $	$-3.7\% \\ +16.3\%$
Location	$\Delta M_{fa} \ \Big $	ΔM_{ss}	ΔM_{yaw}
Tower bottom	-1.6%	-0.5%	-0.7%

Table 3.2: Relative changes in extreme loads at blade root and tip joint, as well as tower bottom

3.5 Effect of blade sweep on fatigue loads

Similar to the analysis presented in Section 3.4, the influence of blade sweep on the fatigue loads can be investigated. For this purpose, simulations are run according to DLC 1.2 defined by the IEC standard [24]. This DLC represents the turbine in power production under normal turbulence. Again, multiple random wind seeds are run per wind speed, and each simulation lasts $600\,\mathrm{s}$ plus an initial $40\,\mathrm{s}$ start-up period omitted in the final processing. Per wind speed and random seed, a damage-equivalent load (DEL) is calculated using a rainflow counting algorithm on the flapwise, edgewise and torsional moment signals at blade root and tip joint as well as the fore-aft, side-side and yawing moments at the tower bottom [26]. A Wöhler exponent of m=10 for the blade loads, m=4 for the tower loads [27], and a number of reference cycles $N_{ref}=10^7$ are used.

Figure 3.8 (a) - (c) shows the flapwise, edgewise and torsional DEL at the blade root averaged per wind speed over the random wind seeds. The flapwise DEL generally increase with increasing wind speed, except for a saddle area around the rated wind speed. Leading up to the saddle, the turbine's rotor speed is driven by the wind velocity. With increasing wind speed, the magnitude of wind speed variations also increases. This entails changes in rotor speed and flapwise loading, leading to the initial steep rise in flapwise DEL. Around rated, the controller regulates the rotor speed to be more constant, thus reducing the fatigue loading. Beyond the saddle, the ever-larger variations in wind speed outweigh the controller's ability to reduce rotor speed variations so that the DEL rise again. The edgewise blade root DEL are dominated by the gravitational loads and, thus, by the rotor speed. This explains why the DEL curve flattens beyond rated conditions. For very high wind speeds, the pitch angle is also high so that the edgewise loads are more aligned with the wind direction. This leads to a slight increase in edgewise DEL for very high wind speeds. The torsional fatigue loads exhibit a minimum around rated conditions. The negative slope leading up to the rated wind speed is a consequence of flapwise blade prebend. This prebend entails a strong correlation of the torsional blade loads and the rotor azimuth due to gravity. With increasing wind speed, the rotor loading causes the blades to straighten out, and the gravitational contribution to the torsional blade root moment diminishes. Beyond rated conditions, the pitching rate increases. This, in combination with gravitational loads due to the blade bending towards the tower, causes the positive DEL slope for higher wind speeds. The DEL of the straight and swept blade configuration exhibit very similar trends. However, both flapwise and torsional blade root DEL reduce slightly when sweeping the blade tip. The edgewise DEL are practically identical.

Figure 3.8 (d) – (f) shows the DEL at the tip joint. In flapwise direction, the same trend as at the blade root can be observed. In edgewise direction, the DEL rise monotonously with increasing wind speed rather than plateauing as at the blade root. At the tip joint, gravitational loads are less dominant than at the root and aerodynamic loads contribute relatively more to the fatigue loading. Therefore, the edgewise DEL are driven by the increasing magnitude of velocity

TNO Public 17/24

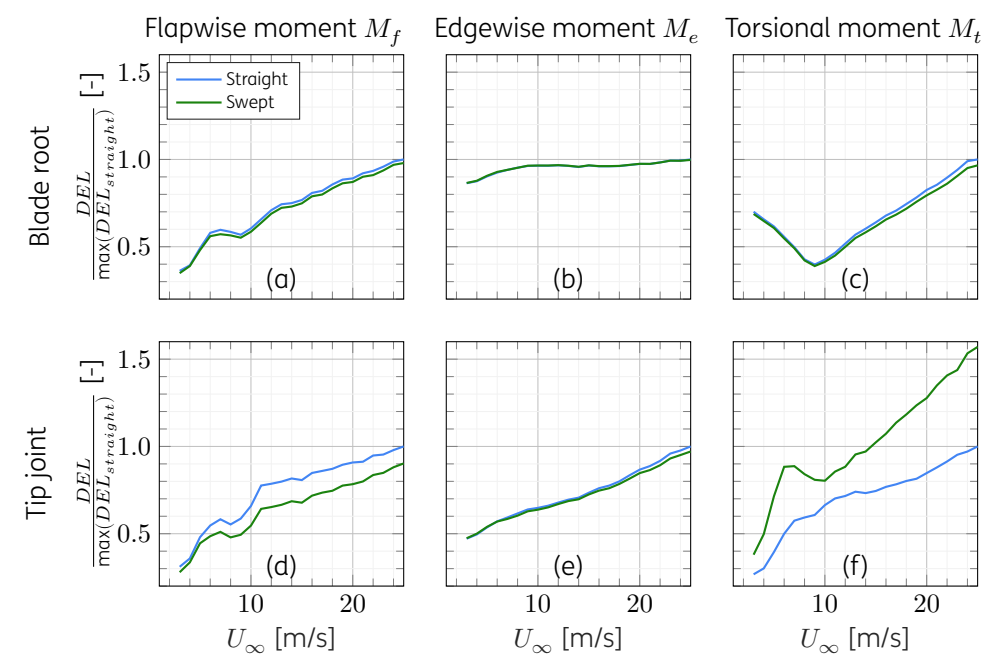


Figure 3.8: Normalised flapwise, edgewise and torsional DEL at the blade root and tip joint as a function of wind speed for the straight and swept case

variations with increasing wind speed. The same holds for the torsional tip joint DEL of the straight blade. While the blade root experiences dominant gravitational loads due to blade prebend, their influence is relatively lower than that of the variable aerodynamic loads due to changes in wind speed. The torsional DEL of the swept blade differ significantly from the straight blade. The fatigue loads increase and follow a pattern closely related to the flapwise DEL, further corroborating the coupling of flapwise bending and torsional deformations. The increased torsional DEL are a sign that the blade passively twists due to unsteady inflow conditions, leading to the relatively substantial reduction of flapwise fatigue loads as seen in Figure 3.8 (d). In edgewise direction, a minor sweep-induced decrease of DEL can be seen for very high wind speeds.

The DEL of the fore-aft, side-side and yawing moment at the tower bottom are given in Figure 3.9. The fore-aft DEL are closely related to rotor thrust and, thus, exhibit a pattern very similar to the blade root flapwise DEL. The side-side and yawing DEL are dominated by the increasing magnitude of wind speed variations with increasing wind speed. However, just below rated conditions, there is an apparent tower excitation in the side-side direction by the rotational frequency. This leads to a local maximum before returning to the approximately linear relation to the wind speed. In terms of sweep-induced relative change, the tower bottom DEL show minor reductions in the fore-aft and yawing direction and negligible differences in the side-side direction.

By multiplying the DEL per wind speed with the expected wind speed probability distribution, a lifetime DEL is determined. The wind speed probability distribution is a Rayleigh distribution defined by

 $F(U_{\infty}) = 1 - \exp\left(-\pi \left(\frac{U_{\infty}}{2\,U_{ave}}\right)^2\right) \tag{3.2}$

with an annual average wind speed $U_{ave}=8.5\,\mathrm{m/s}$ and the characteristic turbulence intensity is $TI=14\,\%$ in accordance with IEC standard 61400-1 for turbine class IIB.

TNO Public 18/24

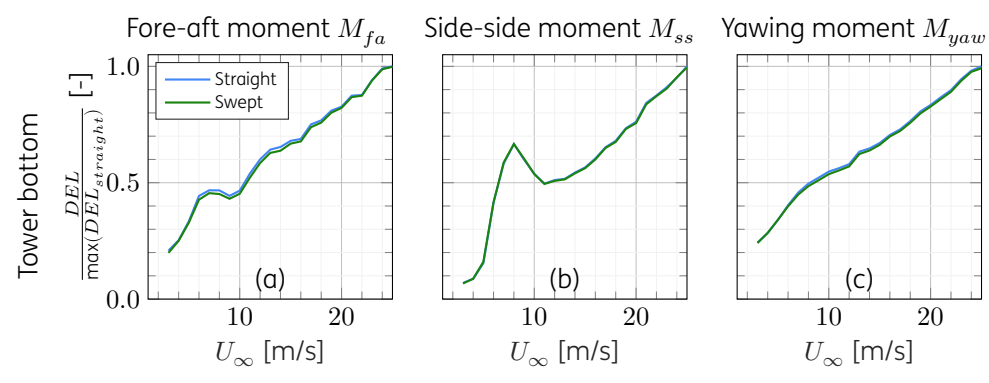


Figure 3.9: Normalised fore-aft, side-side and yawing DEL at the tower bottom as a function of wind speed for the straight and swept case

A summary of the relative changes in lifetime DEL is presented in Table 3.3. Flapwise DEL decrease throughout the blade. The relative decrease is higher at the tip joint than at the blade root, which can be explained by the overall decreasing load level with increasing spanwise position. The torsional DEL follow this trend at the blade root, where considerable load reductions are achieved. However, a strong increase of torsional DEL occurs at the tip joint. This is expected, as the objective of sweep is to passively twist the blade as a reaction to changing inflow conditions. This effect is felt most in the region where sweep is applied. Edgewise DEL are hardly sensitive to the application of blade sweep. The tower bottom fore-aft and yawing DEL decrease while there is a negligible increase in the side-side direction.

Location	$\Delta \mathrm{DEL}(M_f)$	$\Delta {\rm DEL}(M_e)$	$\Delta \mathrm{DEL}(M_t)$
Blade root Tip joint	$\begin{array}{c c} -2.6\% \\ -15.0\% \end{array}$	$\begin{array}{c c} +0.1\% \\ -1.9\% \end{array}$	$^{-3.0\%}_{+43.2\%}$
Location	$\Delta \mathrm{DEL}(M_{fa})$	$\Delta { m DEL}(M_{ss})$	$\Delta {\rm DEL}(M_{yaw})$
Tower bottom	-2.1%	+0.1 %	-1.4%

Table 3.3: Relative changes in lifetime DEL at blade root and tip joint, as well as tower bottom

3.6 Effect of blade sweep on energy production

The simulation results of DLC 1.2 also yield the rotational speed, pitch angle and generated power as a function of wind speed. As such, it can be evaluated how the swept blade tip affects the turbine performance. For each wind speed, these quantities are averaged over the simulation duration and the random seeds. Figure 3.10 shows the resulting normalised curves.

It is evident that the introduction of blade sweep does not lead to changes in the rotational speed. This is expected as both blade configurations are simulated with the same controller and, thus, also identical targeted rotor speeds. While the pitch angle is in close agreement for most wind speeds, minor deviations can be seen for very high wind speeds. Here, the rotor loading and, consequently, the effect of bend-twist coupling are small. Therefore, the twist pre-compensation described in Section 3.2 is too large in these conditions, and the controller increases the pitch angle slightly to compensate.

As a logical consequence, changes in power output due to blade sweep are negligible, too. This is confirmed further when calculating the annual energy production (AEP) by multiplying the

TNO Public 19/24

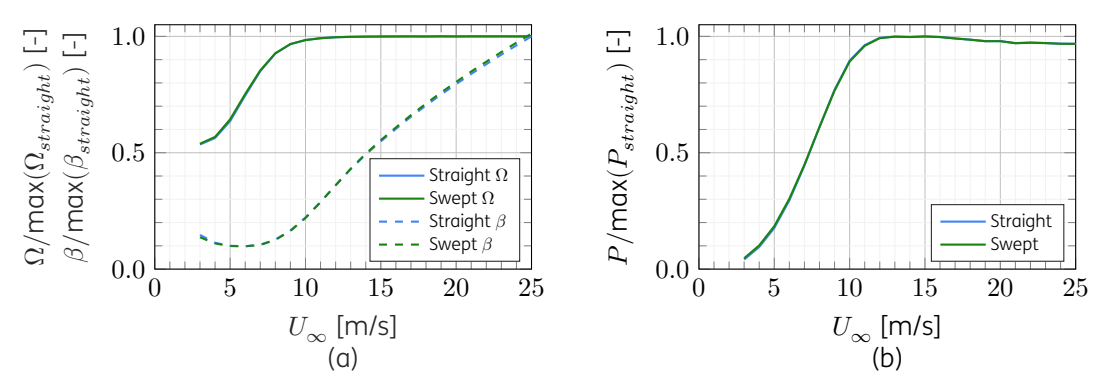


Figure 3.10: Normalised rotational speed and pitch angle curves (a) and power curves (b) of the straight and swept blade configuration

power curves with the wind speed probability distribution given in Equation 3.2 and the hours per year. The sweep-induced relative change in AEP is Δ AEP = +0.26 %.

TNO Public 20/24

4 Conclusions and outlook

This study presents results from numerical investigations aimed at evaluating swept wind turbine blade tip designs and their impact on extreme and fatigue blade loading. These investigations were conducted within the context of the TIADE project, a field measurement campaign on a 3.8 MW research turbine. By conducting this research within the framework of a field experiment, practical implications such as a realistic design space, the accommodation of increased torsional loading and the need for a steady twist compensation to maintain turbine performance could be highlighted.

The design space of the swept tip was defined by geometric and load limitations dictated by this research turbine. More specifically, the sweep starting position was defined by a tip joint designed to allow different tip geometries to be mounted. This already existing tip joint was engineered to withstand the loads of a straight blade tip. A load margin was generated by reducing the rated rotor speed within the simulations to accommodate the additional torsional loads due to sweep-induced bend-twist coupling. The maximally swept tip geometry within these load restrictions was defined by a sweep starting position of $z_{start}\,=\,0.8\,R$ and a tip sweep of $y_{tip}\,=\,-0.02\,R.$

By simulating DLC 1.2 and DLC 1.3 as defined by IEC standard 61400-1, the impact of the swept tip on fatigue and extreme loads during power production was evaluated. This detailed analysis investigated the loads as a function of the wind speed. As such, it contributes to an increased understanding of how blade sweep alters a wind turbine blade's aeroelastic characteristics.

Flapwise extreme loads were shown to reduce throughout the blade, with higher relative reductions with increasing radial position, where the absolute blade loading is smaller. Torsional extreme loads are reduced at the blade root but increased at the tip joint location where the bend-twist coupling is strongest. Edgewise extreme loads remained largely unaffected by the application of blade sweep. The extreme fore-aft, side-side and yawing moments at the tower bottom all reduce, with the most significant reduction in the fore-aft direction.

The sweep-induced changes in damage-equivalent loads followed a similar pattern as the extreme loads. Again, flapwise DEL reduced throughout the blade with a higher relative impact in the outboard region. Torsional DEL also reduced at the blade root but increased at the tip joint. Edgewise DEL were hardly sensitive to the swept blade tip. The tower bottom DEL exhibited reductions in the fore-aft and torsional direction, while a negligible increase occurred in the side-side direction.

Finally, it was demonstrated that the power curve and, consequently, the annual energy production were unaffected by the swept blade geometry. This indicates that rotor loads can be reduced even within limited blade sweep design space without sacrificing rotor performance. As such, the potential of swept tips as a retrofit option for segmented blades is highlighted.

Future research should aim at experimentally validating these numerical simulation results on a multi-megawatt turbine scale. Furthermore, the numerical investigations should be expanded to a broader design space not limited by project restrictions. This way, the positive

TNO Public 21/24

) TNO Public) TNO 2025 R10229

effects of blade sweep demonstrated in this study can likely be maximised and motivate the application of blade sweep to new generations of lighter and, thus, cheaper wind turbine blades.

TNO Public 22/24

References

- [1] P. Veers et al. "Grand challenges in the science of wind energy". In: *Science* 366.6464 (Oct. 2019). Publisher: American Association for the Advancement of Science, eaau2027. DOI: 10.1126/science.aau2027.
- [2] M. Zuteck. Adaptive blade concept assessment: Curved platform induced twist investigation. SAND2002-2996. Office of Scientific and Technical Information (OSTI), Oct. 2002. DOI: 10.2172/803289.
- [3] S. Larwood and M. Zuteck. "Swept wind turbine blade aeroelastic modeling for loads and dynamic behavior". In: AWEA Windpower. AWEA Windpower, Jan. 2006.
- [4] T. Ashwill, G. Kanaby, K. Jackson, and M. Zuteck. "Development of the sweep-twist adaptive rotor (STAR) blade". In: 48th AIAA aerospace sciences meeting including the new horizons forum and aerospace exposition. American Institute of Aeronautics and Astronautics, Jan. 2010. DOI: 10.2514/6.2010–1582.
- [5] T. Barlas, N. Ramos-García, G.R. Pirrung, and S. González Horcas. "Surrogate-based aeroelastic design optimization of tip extensions on a modern 10 MW wind turbine". English. In: *Wind Energy Science* 6.2 (Mar. 2021). Publisher: Copernicus GmbH, pp. 491–504. ISSN: 2366-7443. DOI: 10.5194/wes-6-491-2021.
- [6] T. Barlas et al. "Wind tunnel testing of a swept tip shape and comparison with multifidelity aerodynamic simulations". In: Wind Energy Science 6.5 (Oct. 2021). Publisher: Copernicus GmbH, pp. 1311–1324. DOI: 10.5194/wes-6-1311-2021.
- [7] T. Barlas et al. "Atmospheric rotating rig testing of a swept blade tip and comparison with multi-fidelity aeroelastic simulations". English. In: Wind Energy Science 7.5 (Oct. 2022). Publisher: Copernicus GmbH, pp. 1957–1973. ISSN: 2366-7443. DOI: 10.5194/wes-7-1957-2022.
- [8] E. Fritz, K. Boorsma, and C. Ferreira. Experimental analysis of a horizontal axis wind turbine with swept blades using PIV data. English. in review. Jan. 2024. DOI: 10.5194/wes-2024-11.
- [9] A. Li et al. "Fast trailed and bound vorticity modeling of swept wind turbine blades". In: Journal of Physics: Conference Series 1037 (June 2018). Publisher: IOP Publishing, p. 062012. DOI: 10.1088/1742-6596/1037/6/062012.
- [10] A. Li et al. "A computationally efficient engineering aerodynamic model for swept wind turbine blades". In: *Wind Energy Science* 7.1 (Aug. 2021). Publisher: Copernicus GmbH, pp. 129–160. DOI: 10.5194/wes-2021-96.
- [11] E. K. Fritz, C. Ferreira, and K. Boorsma. "An efficient blade sweep correction model for blade element momentum theory". en. In: *Wind Energy* 25.12 (2022), pp. 1977–1994. ISSN: 1099-1824. DOI: 10.1002/we.2778.
- [12] S. G. Horcas et al. "Comparison of aerodynamic models for horizontal axis wind turbine blades accounting for curved tip shapes". en. In: *Wind Energy* 26.1 (2023), pp. 5–22. ISSN: 1099-1824. DOI: 10.1002/we.2780.
- [13] D. R. Verelst and T. J. Larsen. Load consequences when sweeping blades A case study of a 5 MW pitch controlled wind turbine. English. RISO-R-1724(EN). Technical University of Denmark, Risø National Laboratory for Sustainable Energy. Wind Energy Division, Roskilde (Denmark), 2010.
- [14] M. Hansen. "Aeroelastic properties of backward swept blades". In: 49th AIAA aerospace sciences meeting including the new horizons forum and aerospace exposition. American Institute of Aeronautics and Astronautics, Jan. 2011. DOI: 10.2514/6.2011-260.

TNO Public 23/24

- [15] S. Larwood, C. van Dam, and D. Schow. "Design studies of swept wind turbine blades". In: Renewable Energy 71 (Nov. 2014), pp. 563–571. DOI: 10.1016/j.renene.2014.05.050.
- [16] N. M. Karaolis, P. J. Musgrove, and G. Jeronimidis. "Passive aerodynamic control using composite blades". English. In: *Use of composite materials for wind turbines workshop, Harwell, UK. Jan.* 1988.
- [17] M. Capellaro. "Design Limits of Bend Twist Coupled Wind Turbine Blades". en. In: 53rd AIAA/ASME/ASCE/AHS/ASC Structures, Structural Dynamics and Materials Conference & 20th AIAA/ASME/AHS Adaptive Structures Conference & 14th AIAA. Honolulu, Hawaii: American Institute of Aeronautics and Astronautics, Apr. 2012. ISBN: 978-1-60086-937-2. DOI: 10.2514/6.2012-1501.
- [18] S. F. Hoerner. Fluid-dynamic lift. Published by Liselotte A. Hoerner, 1985.
- [19] E. Fritz, K. Boorsma, and C. Ferreira. "Validation of a BEM correction model for swept blades using experimental data". In: *Journal of Physics: Conference Series* (2024). in review.
- [20] T. Burton, D. Sharpe, N. Jenkins, and E. Bossanyi. *Wind energy handbook 2e.* John Wiley & Sons, June 2011. ISBN: 0-470-69975-2.
- [21] F. Grasso, A. van Garrel, and G. Schepers. "Development and validation of generalized lifting line based code for wind turbine aerodynamics". In: 49th AIAA aerospace sciences meeting including the new horizons forum and aerospace exposition. American Institute of Aeronautics and Astronautics, Jan. 2011. DOI: 10.2514/6.2011-146.
- [22] C. Lindenburg. PHATAS User's manual version 11737. WMC-2016-005. (Confidential). LM Wind Power, 2020.
- [23] H. Snel, R. Houwink, and T. Bosscher. Sectional prediction of lift coefficients on rotating wind turbine blades in stall. ECN-C-93-052. Energy Research Center of the Netherlands, 1994.
- [24] International Electrotechnical Commission. Wind turbines part 1: Design requirements (IEC 61400-1:2005(E)). 2005.
- [25] E. Gaertner et al. Definition of the IEA wind 15-megawatt offshore reference wind turbine Tech. Rep. 2020.
- [26] H. Hendriks and B. Bulder. Fatigue Equivalent Load Cycle Method. A General Method to Compare the Fatigue Loading of Different Load Spectrums. ECN-C-95-074. Energy Research Center of the Netherlands, 1995.
- [27] N. Dimitrov, A. Natarajan, and J. Mann. "Effects of normal and extreme turbulence spectral parameters on wind turbine loads". In: *Renewable Energy* 101 (Feb. 2017), pp. 1180–1193. ISSN: 0960-1481. DOI: 10.1016/j.renene.2016.10.001.

TNO Public 24/24

Energy & Materials Transition

Westerduinweg 3 1755 LE Petten www.tno.nl

